Journal of Natural Gas Science and Engineering xxx (2016) 1–9

Contents lists available at ScienceDirect

Journal of Natural Gas Science and Engineering

journal homepage: www.elsevier.com/locate/jngse

Numerical modeling of cryogenic fracturing process on laboratory-scale Niobrara shale samples

Bowen Yao*, Lei Wang, Xiaolong Yin, Yu-Shu Wu

Petroleum Engineering Department, Colorado School of Mines, USA

ARTICLE INFO

Article history:
Received 31 August 2016
Received in revised form
14 October 2016
Accepted 22 October 2016
Available online xxx

Keywords:
Cryogenic fracturing
Stimulation
Simulation
Thermal stress
tri-axial stress

ABSTRACT

Cryogenic fracturing is a new fracturing concept that uses cryogenic fluids as fracturing fluids. Its mechanism rests on the effect of a thermal shock (sharp thermal gradient) introduced by cryogen on the hot surface of reservoir rock. Fractures can then be initiated and propagated due to strong local tensile stress. The objective of this research is to simulate the cryogenic fracturing experiments on Niobrara shale samples. The experimental processes are simulated under different conditions and matched with the actual experiment results. The influences of different confining stress, injection pressure and failure criteria are identified by comparing results from modeling and experiments. The simulation tool developed can also predict the distribution of artificial fractured samples.

1. Introduction

Cryogenic fracturing is a new concept that looks to expand and improve on traditional hydraulic fracturing technology. The concept rests on the idea that a cryogenic fluid (such as liquid nitrogen) can induce fractures when brought into contact with a much warmer rock under downhole conditions. The rapid heat transfer, better known as a thermal shock, will cause the surface of the rock to shrink, relative to the inner warmer material of the rock and eventually fail in tension, inducing fractures orthogonal to the contact plane of the cryogen and the rock. Cryogenic fracturing technology could potentially increase the effects of fracturing and decrease the cost of fracturing resulting in more formations becoming economically viable.

The first cryogenic fracturing experiment was conducted by using gelled liquid carbon dioxide to stimulate tight gas sand formations instead of conventional fracturing fluids such as water or oil (King, 1983). All of the wells showed increased production rate after treatment. To further address the fracturing mechanism, McDaniel et al. (1998) conducted several laboratory liquid nitrogen submersion tests on coal samples to prove that cryogenic fracturing may have an advantageous effect on gas production from tight, low-rate coal-bed methane wells. They also applied cryogenic fracturing to 5 wells for field tests, which showed mixed results: three of them experienced increased production rate, one experienced equivalent production and one experienced decreased production. Among the three wells with increased production, two of them had long term increment in production. Grundmann et al. (1998) conducted later a cryogenic fracturing treatment in a Devonian shale well with liquid nitrogen. The well showed an 8% increment in the initial production rate when compared to a nearby offset well that underwent a traditional nitrogen gas fracturing treatment.

Thermally induced fracturing is one of the most important phenomenon during cryogenic fracturing. Although it is well established in rock mechanics, the focus of previous studies are mostly on high temperature rock failure, such as thermal spalling and thermal pressurization by pore fluid. Very few studies were conducted for rock failure at low temperature. The most simplified model for thermally induced fracturing during water injection is simply assume the fracturing pressure of the rock to be equal to the minimum stress with thermal effect (Detienne et al., 1998). Zoback (2007) presented a failure criterion for fracture initiation coupled with thermal effect as:

$$p_b = 3\sigma_{h\min} - \sigma_{H\max} - p_p - \sigma^{\Delta T} \quad (1)$$

where:

* Corresponding author.
E-mail address: byao@mines.edu (B. Yao).

http://dx.doi.org/10.1016/j.jngse.2016.10.041
1875-5100/

p_b is the formation break down pressure;
$\sigma_{h\min}$ is the minimum horizontal stress;
$\sigma_{H\max}$ is the maximum horizontal stress;

p_p is the pore pressure;

$\sigma^{\Delta T}$ is the thermo-elastic stress.

Luo and Bryant (2010) adapted this criterion and applied it to a research on CO_2 injection induced fractures. Zhou et al. (2010) studied the initiation, propagation and interaction of thermal failures within impermeable, hot and dry rocks due to the cooling of a main hydraulic fracture by long-term reservoir fluids circulation, combining thermo-elastic model (Jaeger et al., 2009) and stress intensity factor (Olson and Pollard, 1991).

The objective for this study is to model and evaluate the experimental cryogenic fracturing treatments on Niobrara shale samples. The fracturing process at low temperature of rock samples during cryogenic treatment are simulated and matched with experiment results. The simulation tool is capable of predicting the fracture distribution. In addition to previous studies, the influences of different confining stresses and injection pressure are identified. This study also provides valuable guidance to potential field applications of cryogenic fracturing technology.

1.1. Theoretical analysis

1.1.1. Heat transfer and fluid flow model

For an arbitrary control volume with arbitrary shape, the governing equation for mass and heat balance according to Fakcharoenphol et al. (2013) can be written in the form:

$$\frac{d}{dt}\int_{V_n} Q^{\kappa} dV_n = \int_{\Gamma_n} F^{\kappa}\cdot\vec{n}\, d\Gamma_n + \int_{V_n} q^{\kappa} dV_n \tag{2}$$

where:

$\kappa = 1, \ldots, NK$ (total number of components);
$n = 1, \ldots, NEL$ (total number of grid blocks);
V_n is an arbitrary subdomain of the system under study;
Γ_n is the closed surface by which the subdomain is bounded by;
Q is the quantity represents mass or energy per volume;
F is mass or heat flux;
q is sinks and sources;

$\vec{n}$ is a normal vector on surface element $d\Gamma_n$ pointing inward into V_n.

1.1.2. Thermoelastic model

Thermal stress is the stress change caused by temperature change within a solid material. It is the most important parameter when simulating the cryogenic fracturing process. The thermally induced stress can be integrated into the generalized stress-strain relation in a rock volume (Zoback, 2007), as shown below:

$$\sigma_{kk} - B_i \times p_p - \frac{E}{(1-2\nu)}[\beta(T-T_0)] = \frac{E}{(1+\nu)}\varepsilon_{kk} + \frac{E}{(1+\nu)(1-2\nu)}(\varepsilon_{xx}+\varepsilon_{yy}+\varepsilon_{zz}) \tag{3}$$

Where:

σ is the normal stress;
ε is the strain;

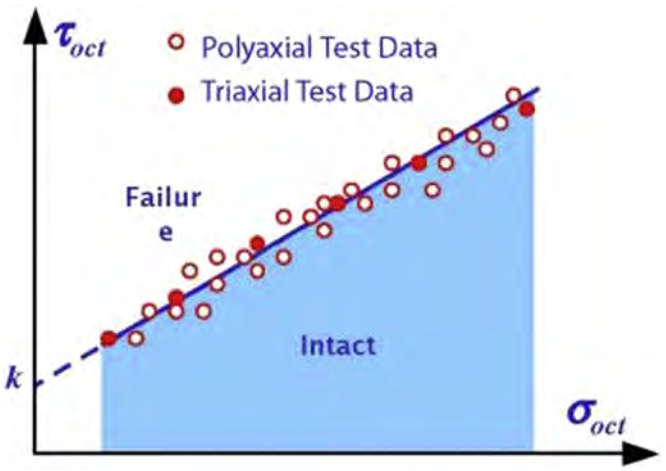

Fig. 1. Failure envelope of Mogi - Coulomb criterion by Aadnoy and Looyeh (2011).

Subscript kk is direction, which can be x, y and z;
B_i is the Biot number of the rock;
β is the linear thermal expansion of the rock;
E is the Young's modulus;
ν is the Poisson's ratio;
p_p is the pore pressure;
T is the current temperature;
T_0 is the reference or original temperature.

1.1.3. Rock failure criteria

A failure criterion is used to judge the condition of rock fracturing. It gives the maximum strength of rock under certain stress conditions. Once the stress exceeds the maximum strength given by the failure criterion, the rock will break, in other words, be fractured. The current failure model used in this simulating tool is the Mogi − Coulomb Failure Criterion, which is first introduced by Al-Ajmi and Zimmerman (2006) and widely used in rock mechanics. The Mogi − Coulomb Failure Criterion has the following

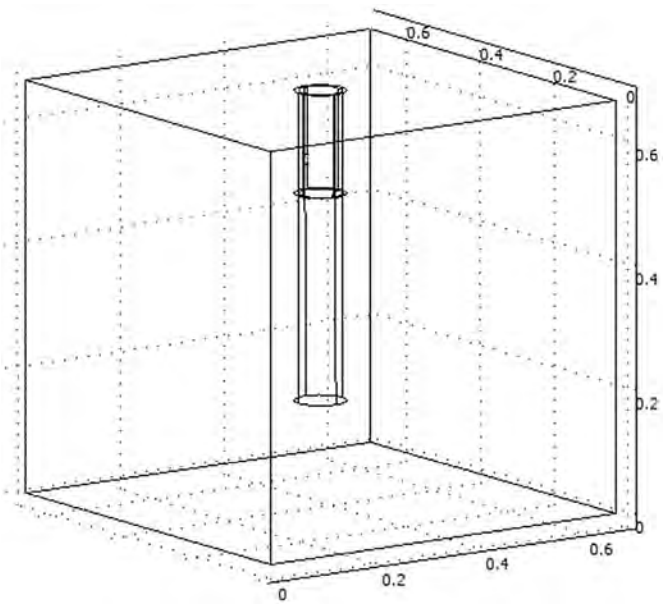

Fig. 2. Schematic drawing for modeling geometry.

Please cite this article in press as: Yao, B., et al., Numerical modeling of cryogenic fracturing process on laboratory-scale Niobrara shale samples, Journal of Natural Gas Science and Engineering (2016), http://dx.doi.org/10.1016/j.jngse.2016.10.041

Table 1
Input parameters for simulation.

Properties	Value
Ambient Pressure	11.8 psi (81.4 KPa)
Ambient Temperature	66 °F (19 °C)
Rock Density	2.38 g/cc
Permeability	1.00×10^{-3} mD
Permeability of Fractured Grid	200 mD
Porosity	8%
Rock Compressibility	2×10^{-3} psi^{-1} (2.9×10^{-7} Pa)
Thermal Diffusivity	8×10^{-7} m^2/s
Thermal Expansion Coefficient	2.7×10^{-5} °C
Specific Heat	990 J/(kg K)
Young's Modulus	7.15×10^6 psi (4.93×10^4 Mpa)
Poisson's Ratio	0.268
Mogi-Coulomb Constant, k	230 psi (1.59 Mpa)
Mogi-Coulomb Slope, m	0.58

form:

$$\tau_{oct} = k + m\sigma_{oct} \tag{4}$$

where:

τ_{oct} is the octahedral shear stress;
σ_{oct} is the octahedral normal stress;
k is the Mogi-Coulomb intercept;
m is the Mogi-Coulomb slope.

The octahedral shear and normal stresses are defined as:

$$\tau_{oct} = \frac{1}{3}\sqrt{(\sigma_v - \sigma_{H\max})^2 + (\sigma_v - \sigma_{h\min})^2 + (\sigma_{H\max} - \sigma_{h\min})^2}$$
$$\sigma_{oct} = \frac{1}{3}(\sigma_v + \sigma_{H\max} + \sigma_{h\min}) \tag{5}$$

where:

σ_v is the vertical stress;
$\sigma_{h\min}$ is the minimum horizontal stress;
$\sigma_{H\max}$ is the maximum horizontal stress.

In the above equations, k and m are constants that are usually obtained from fitting actual data. The failure envelope from Mogi–Coulomb Failure Criterion is as shown in Fig. 1. Normally the stress conditions of rock make the calculated τ_{oct} and σ_{oct} fall into the blue area under the failure envelope. When the stress condition changes, i.e. due to cryogenic treatment, the calculated τ_{oct} and σ_{oct} may fall onto a point outside of the failure envelope, the rock would then be fractured. Mogi − Coulomb Failure Criterion is simple and easy to adapt in simulation and has similar accuracy with other failure criteria when assuming that the physical properties of rock

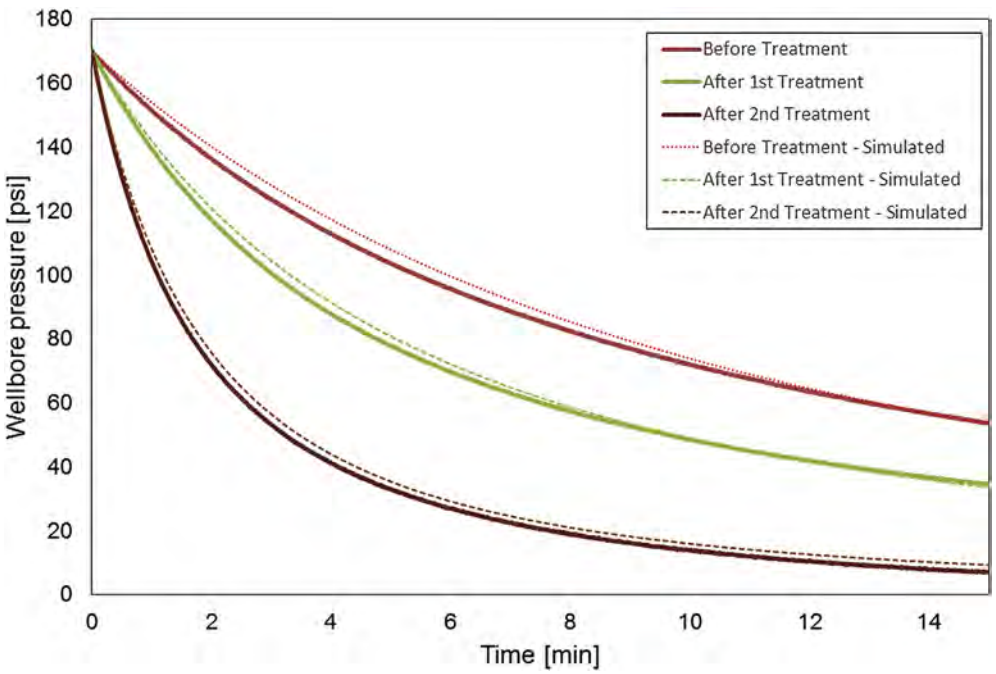

Fig. 3. Pressure decay tests for S1.

Table 2
Experiment and simulation results for S1.

Procedure	Experiment		Simulation		
	Average Permeability	Improvement	Average Permeability	Improve-ment	Fracture Half-length
Before treatment	1.30×10^{-3} mD	1.00	1.00×10^{-3} mD	1.00	0
After low pressure circulation for 40 min	1.65×10^{-3} mD	1.26	1.30×10^{-3} mD	1.30	0.6 in. (1.52 cm)
After 3 cycles of high pressure injection	3.45×10^{-3} mD	2.64	2.25×10^{-3} mD	2.25	0.9 in. (2.29 cm)

Please cite this article in press as: Yao, B., et al., Numerical modeling of cryogenic fracturing process on laboratory-scale Niobrara shale samples, Journal of Natural Gas Science and Engineering (2016), http://dx.doi.org/10.1016/j.jngse.2016.10.041

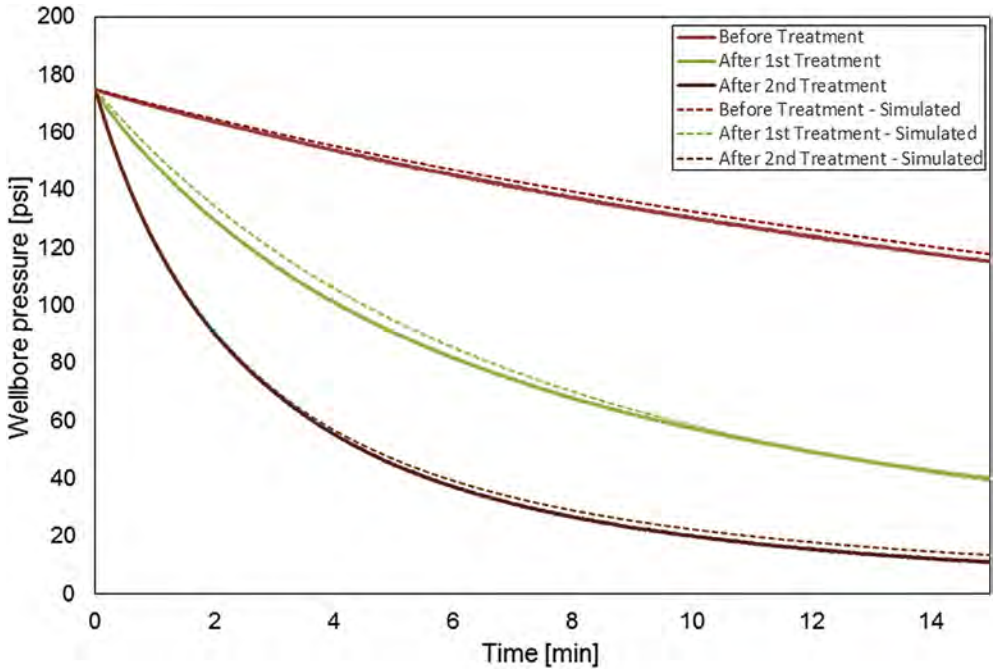

Fig. 4. Pressure decay tests for S2.

Table 3
Experiment and simulation results for S2.

Procedure	Experiment		Simulation		
	Average Permeability	Improvement	Average Permeability	Improvement	Fracture Half-length
Before treatment	2.90×10^{-4} mD	1	1.00×10^{-3} mD	1	0
After 1st round of 3 cycles of high pressure injection	1.25×10^{-3} mD	4.32	3.80×10^{-3} mD	3.8	0.8 in. (2.03 cm) in y 0.4 in. (1.02 cm) in x
After 2nd round of 3 cycles of high pressure injection	2.90×10^{-3} mD	10	6.10×10^{-3} mD	6.1	1 0.2 inch (3.05 cm) in y 0.5 in. (1.27 cm) in x

remain the same with temperature change.

1.2. Numerical modeling

The simulation tool is modified from TOUGH2-EGS (Enhanced Geothermal System) (Fakcharoenphol et al., 2013; Xiong et al., 2013; Zhang et al., 2015, 2016), which is a coupled geomechanical simulator for fluid and heat flows in an enhanced geothermal system. With the ability of TOUGH2-EGS and modification on fracture initiation and propagation, this simulation tool can simulate cryogenic fracturing processes and predict the distribution of fractures.

Fig. 5. Fracture plane of S2 (Wang et al., 2016).

In order to simplify the development of the simulation tool, several assumptions have been made:

- For heat transfer, only heat conduction is considered within each grid. In porous media, the contacting area between fluid and rock surfaces is very large per unit volume of fluid. This indicates that heat conduction plays a much more important role than advection and radiation during a short period of cryogenic treatment. In each grid block, the temperature of the rock matrix is always the same as that of the fluid in the pore volume.
- For fracturing processes, the stress change in the rock matrix includes thermal expansion or contraction due to the change in temperature, fluid pressure in pores, and external stress condition, as imposed by the hydraulic press and pistons in the experiment. The principal stress directions follow the loading direction in the tri-axial experiments.
- The rock matrix is assumed to be homogeneous within each grid block. The heterogeneity of the sample is achieved by assigning different rock properties to different grid blocks.
- For natural fractures, since they are very difficult to characterize, pre-existing natural fractures are neglected. Only the fractures

Please cite this article in press as: Yao, B., et al., Numerical modeling of cryogenic fracturing process on laboratory-scale Niobrara shale samples, Journal of Natural Gas Science and Engineering (2016), http://dx.doi.org/10.1016/j.jngse.2016.10.041

generated by the cryogenic treatment are considered and tracked.

There are three types of grid blocks used in this simulation tool. The normal grid, which can be considered as the intact rock material, has the same properties with the measured rock properties. The fractured grid has larger permeability due to fractures induced by thermal shock in cryogenic fluid treatment. The other properties remain the same with the normal grid. However, since fluid flow increases with higher permeability in this kind of grid, fractured grid blocks generally appear to be more thermally conductive. The third type of grid is the wellbore grid, which is set to have the same property with void space. If the center of a grid block falls within the borehole space, it is set as wellbore grid.

The basic work flow of the simulation tool follows the original work flow of TOUGH2-EGS with modification on fractured grids judgement according to the Mogi-Coulomb Failure Criterion.

The simulation tool simulates the cryogenic fracturing process using a control volume finite difference method. The basic geometry of the simulated well is the same as that in the experiment: the cryogenic fluid flows into a borehole and cools its surface. Then, the fluid will permeate through the porous medium through the inner surface of the borehole. The domain dimensions are set as 8 inch by 8 inch by 8 inch, identical to the dimension of the sample in the actual experiment.

The details of this case are as follows. The domain is a rock sample cube with outer dimensions 20.32 cm × 20.32 cm × 20.32 cm (8 in. × 8 in. × 8 in.). A 2.54 cm (1 in.) diameter borehole is centrally located on top surface extending 15.24 cm (6 in.) into the block. The upper 5.08 cm (2 in.) section of borehole will be cased, which means no fluid flow through this section into samples. Fig. 2 shows the schematic of geometry for modeling.

The outer boundary, which consists of the six surfaces of the sandstone block, is exposed to ambient pressure and temperature in the laboratory, which are 11.8 psia (81.4 KPa) and 66 °F (19 °C). The sample is initially set at the ambient temperature, which is 66 °F (19 °C). The stress condition is set the same as that in the experiment such that simulation and experiments results can be matched and compared. The permeability of fractured grid is an arbitrary large value relative to the original permeability, since it is extremely difficult to measure the permeability of the near wellbore area of shale samples after treatment. All basic input parameters of the simulation are shown in Table 1.

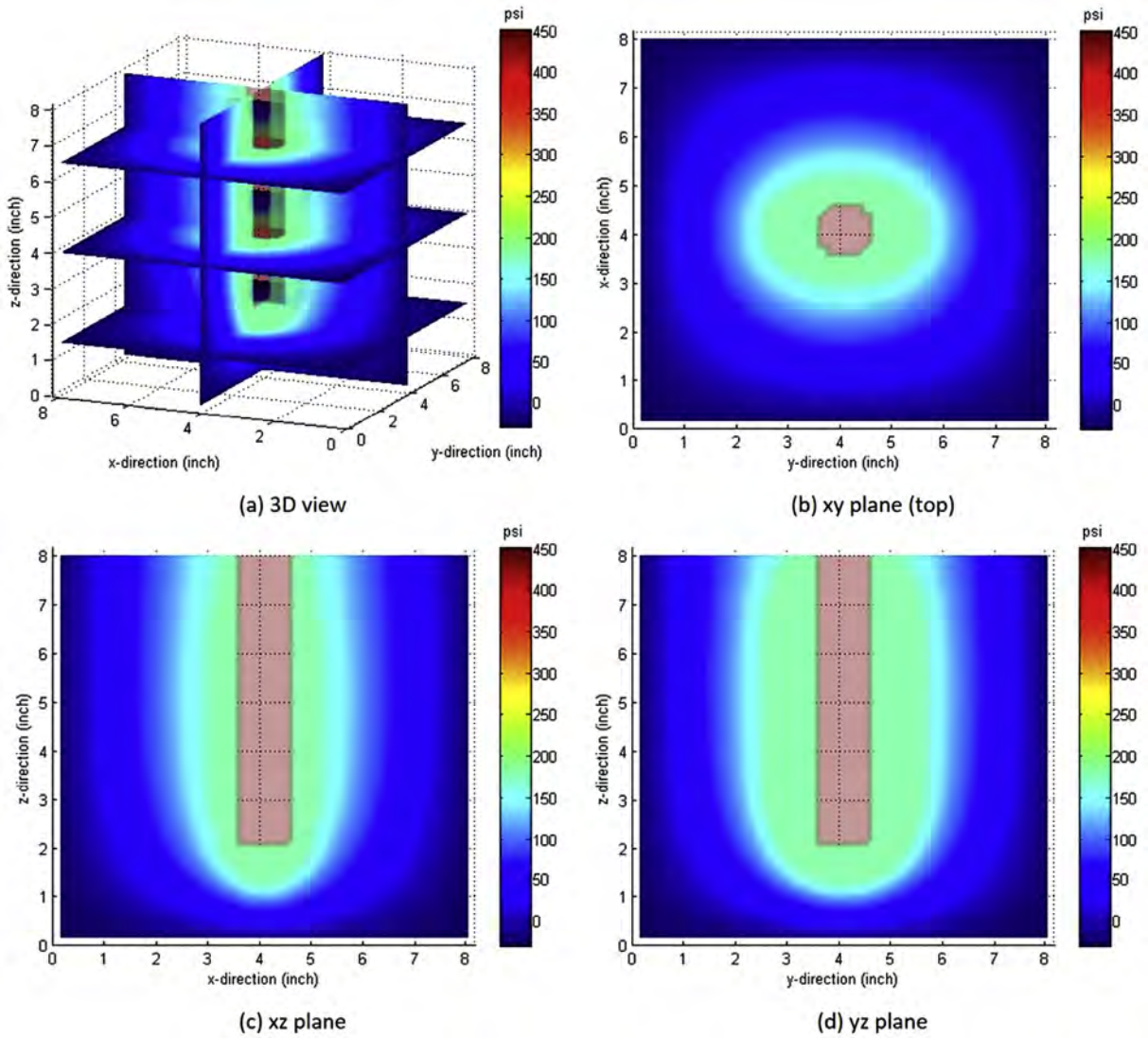

Fig. 6. Pressure distribution in S2 after the second treatment.

Please cite this article in press as: Yao, B., et al., Numerical modeling of cryogenic fracturing process on laboratory-scale Niobrara shale samples, Journal of Natural Gas Science and Engineering (2016), http://dx.doi.org/10.1016/j.jngse.2016.10.041

2. Results

Wang et al. (2016) have tested several Niobrara shale samples with cryogenic fracturing process. The results from simulations are matched and compared with the experiment to evaluate the effect of different test procedures and conditions.

Shale sample # 1 (S1) was treated two rounds with liquid nitrogen under the room temperature. The confining stress profile used for this sample is 1000 psi (6.89 MPa) in x direction, 1500 psi (10.34 MPa) in y direction and 2000 psi (13.79 MPa) in z direction. The first liquid nitrogen treatment is a low-pressure (about 15 psi or 0.1 MPa) circulation and lasts for 40 min. The second treatment includes three cycles of high-pressure liquid nitrogen injection with outlet partially open to provide opportunities for circulation while maintaining a back pressure.

The results of pressure decay tests before and after each treatment is shown in Fig. 3. The average permeability matched from simulation for Shale before the first cryogen treatment is 1.30×10^{-3} mD, after the first treatment is 1.65×10^{-3} mD, and after the second treatment is 3.45×10^{-3} mD. The first round of low-pressure liquid nitrogen circulation increases the average permeability of S1 to 1.26 times to its original value. The second round of high-pressure liquid nitrogen treatment increases the permeability to 2.64 times of its original value. The results of experiment and simulation for S1 are compared side-by-side in Table 2.

Shale sample # 2 (S2) is treated twice with high-pressure liquid nitrogen under the room temperature (Wang et al., 2016). The confining stress profile used for this sample is 1000 psi (6.89 MPa) in x direction, 3000 psi (20.68 MPa) in y direction and 4000 psi (27.58 MPa) in z direction. Both treatment used a pressure of about 450 psi (3.10 MPa) and contained three cycles of liquid nitrogen injection.

The results of pressure decay tests before and after each treatment is shown in Fig. 4. The average permeability matched from simulation for shale before the first cryogen treatment is 2.90×10^{-4} mD, after the first treatment is 1.25×10^{-3} mD, and after the second treatment is 2.90×10^{-3} mD. The first round of high-pressure liquid nitrogen treatment increases the average permeability of S2—4.32 times to its original value. The second round of high pressure liquid nitrogen treatment increases the permeability to 10 times of its original value.

For the second round, distributions of pressure, temperature and fractured grids are shown in Fig. 6, Fig. 7, and Fig. 8,

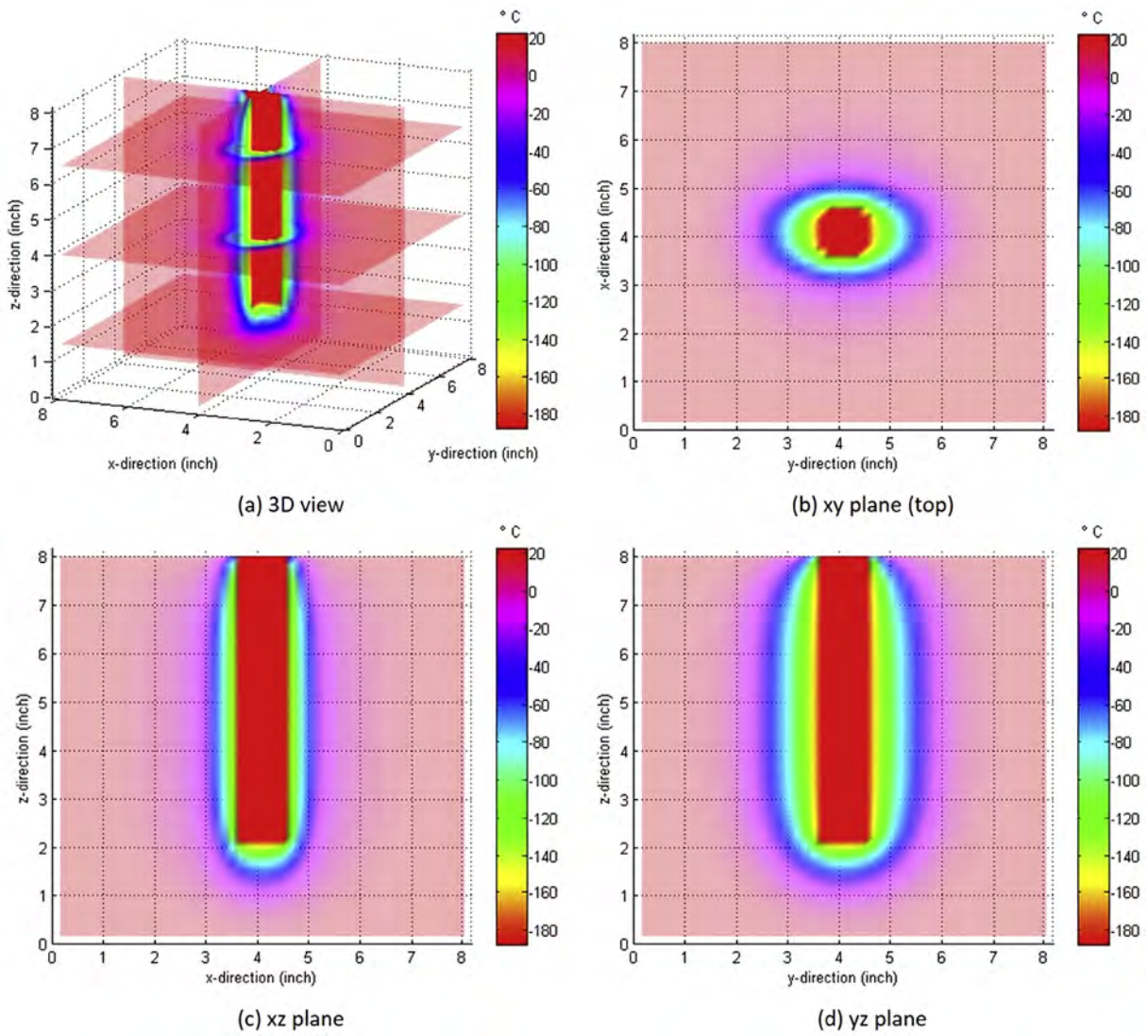

Fig. 7. Temperature distribution in S2 after the second treatment.

Please cite this article in press as: Yao, B., et al., Numerical modeling of cryogenic fracturing process on laboratory-scale Niobrara shale samples, Journal of Natural Gas Science and Engineering (2016), http://dx.doi.org/10.1016/j.jngse.2016.10.041

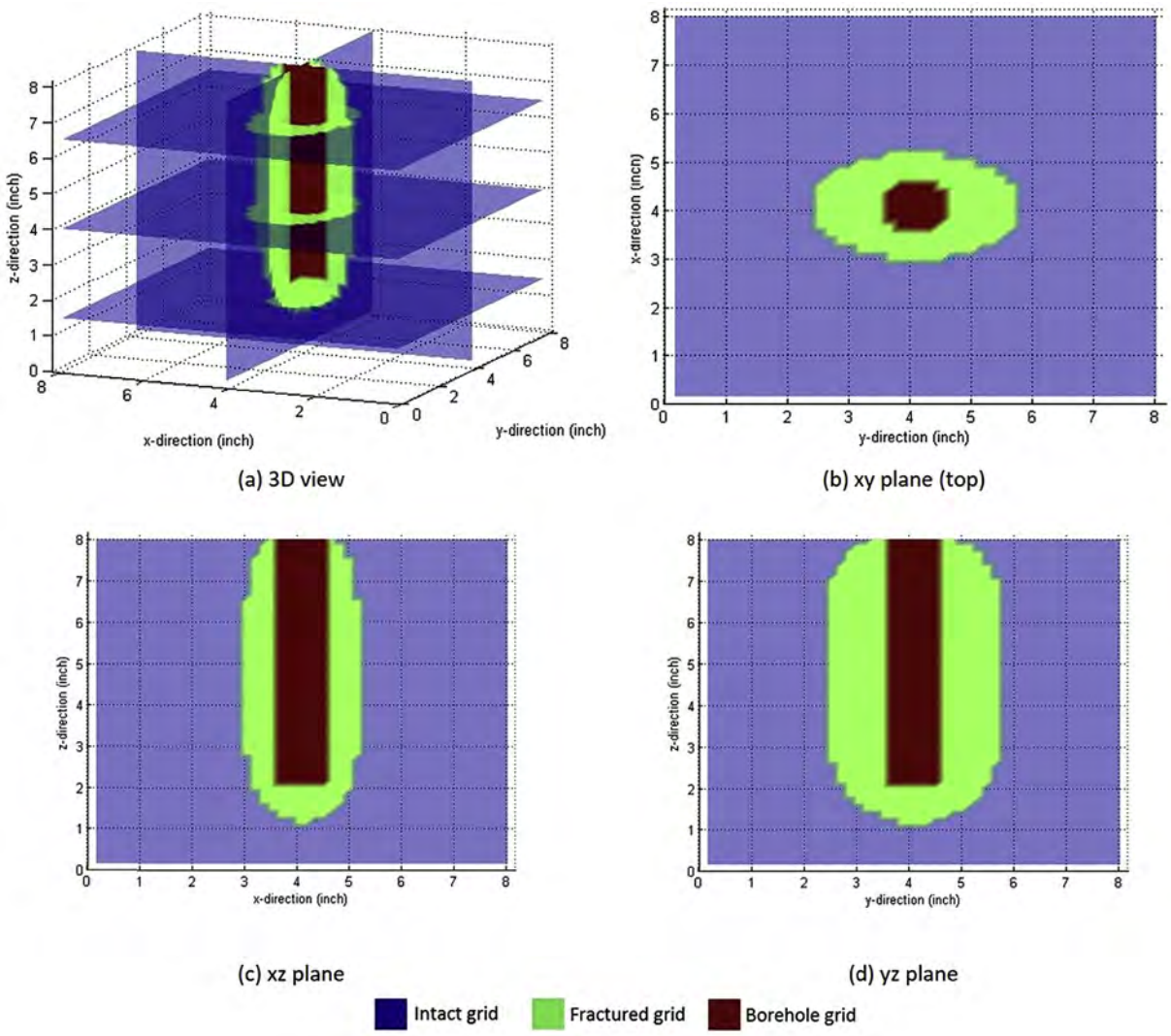

Fig. 8. Fractured grids distribution in S2 after the second treatment.

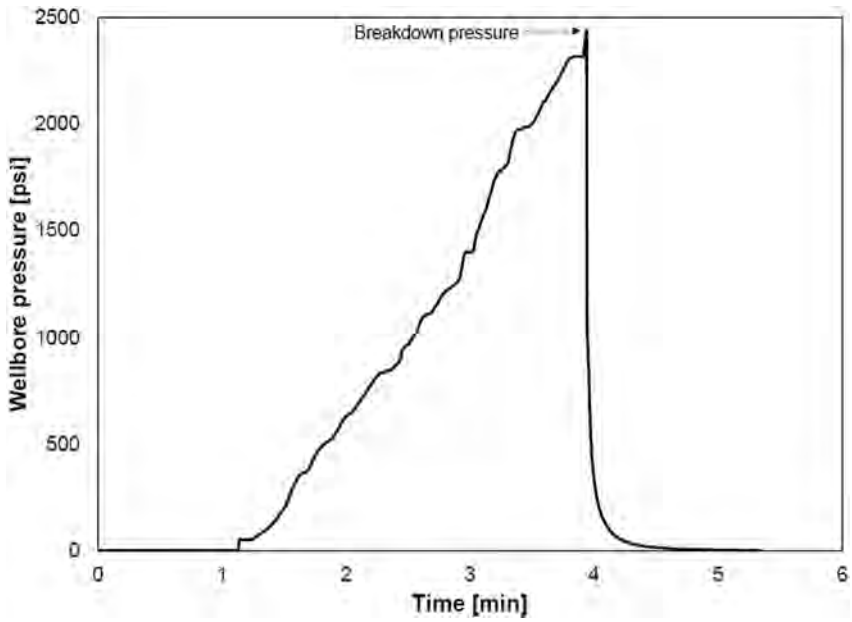

Fig. 9. Breakdown pressure of S4 (Wang et al., 2016).

Please cite this article in press as: Yao, B., et al., Numerical modeling of cryogenic fracturing process on laboratory-scale Niobrara shale samples, Journal of Natural Gas Science and Engineering (2016), http://dx.doi.org/10.1016/j.jngse.2016.10.041

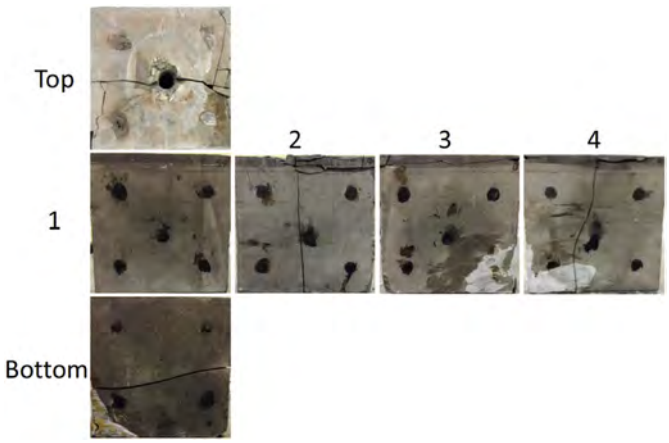

Fig. 10. Sample S4 after fractured by high pressure gas (Wang et al., 2016).

respectively. The fracture half-length after the first treatment is about 0.7 in. (1.24 cm) in y direction and 0.4 inch (1.02 cm) in x direction. The average permeability from simulation is 6.10×10^{-3} mD, which is 6.1 times of its original value. All results of experiment and simulation for S2 are shown in Table 3. Since the base permeability is set as 1.00×10^{-3} mD, which differs from the average permeability of S2 from pressure decay test, the simulation result of this case mainly focuses on the improvement on permeability from the cryogenic treatment instead of matching the permeability. After the cryogen treatment, S2 is fractured with high-pressure gas nitrogen. The section area of fracture plane shows a clear profile for fracture induced by thermal shock, as shown in Fig. 5. By comparing the fracture profile from experiment (Fig. 5) and simulation (Fig. 8), it shows that the simulation is capable for reproducing the experiment and generating reasonable results.

Shale sample # 4 (S4) is directly fractured by high-pressure gas nitrogen to establish a reference for evaluation of cryogenic fracturing efficacy. The confining stress profile used for this sample is 1000 psi (6.89 MPa) in x direction, 1500 psi (10.34 MPa) in y direction and 2000 psi (13.79 MPa) in z direction. The break down pressure for S4 is about 2460 psi (18.2 MPa), which is shown in Fig. 9. Fig. 10 shows pictures of all surfaces of S4 after fractured by high-pressure gas. An observation from the surfaces of S4 is that the facture is in yz plane (surface 2, 4, top and bottom in Fig. 10), which

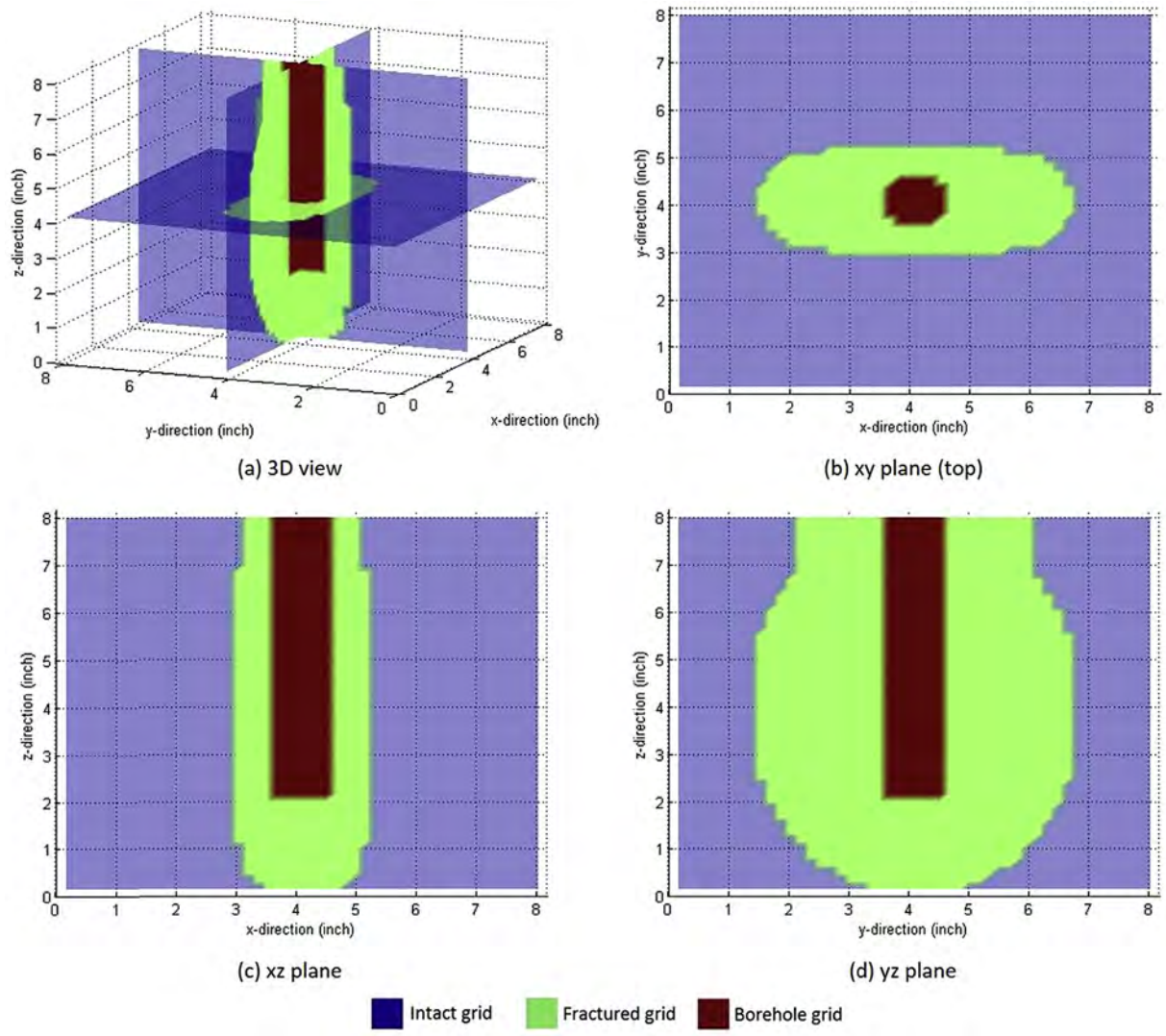

Fig. 11. Fracture distribution in S4.

Please cite this article in press as: Yao, B., et al., Numerical modeling of cryogenic fracturing process on laboratory-scale Niobrara shale samples, Journal of Natural Gas Science and Engineering (2016), http://dx.doi.org/10.1016/j.jngse.2016.10.041

is perpendicular to direction of minimum horizontal stress. A pressure-only (i.e. no cryogen) simulation was run for S4, which provides a fracture distribution as shown in Fig. 11. Fractured grids for this case are mostly distributed in the yz plane, which agrees with the fracture description for S4 mentioned above. Fractures induced by high-pressure nitrogen gas have reached the surfaces on z directions (top and bottom), causing most of gas flow leaks out to ambient environment through these grids. The breakdown pressure for this case is 2472 psi (17.1 MPa), which is very close to the actual breakdown pressure shown in Fig. 9.

3. Conclusions

A simulation tool modified from TOUGH2-EGS is developed for cryogenic fracturing experiment. It can provide predictions that are in good agreement with experiment. The current simulation tool can predict fracture distribution for cryogenic fracturing experiments under different stress conditions. After calibration that is specific to rock type, this simulation tool can provide reasonable fracture profile along with pressure and temperature distributions. The results of the simulation also demonstrates that circulation of cryogenic fluid in wellbore at low pressure can be applied as a near-wellbore formation damage remediation technique with very low cost and without any environmental concerns and high injection pressure tends to enhance cryogenic fracturing process in both speed and fracture conductivity.

Acknowledgement

The authors thank the financial support from Research Partnership to Secure Energy for America from DOE (Development of Non-Contaminating Cryogenic Fracturing Technology for Shale and Tight Gas Reservoirs, Project Number: 10122-20).

Nomenclature

B_i	Biot number of the rock
E	Young's modulus
F	Mass or heat flux
k	Mogi-Coulomb intercept
kk	(subscript) Direction, which can be x, y and z
m	Mogi-Coulomb slope
n	Total number of grid blocks
$\overrightarrow{n}$	A normal vector on surface element $d\Gamma_n$ pointing inward into V_n
p_p	Pore pressure
Q	Quantity represents mass or energy per volume
q	Sinks and sources
T	Current temperature
T_0	Reference or original temperature
V_n	An arbitrary subdomain of the system under study
β	Linear thermal expansion of the rock
ε	Normal strain
Γ_n	Closed surface by which the subdomain is bounded
κ	Total number of components
ν	Poisson's ratio
σ	Normal stress
$\sigma_{H\max}$	Maximum horizontal stress
$\sigma_{h\min}$	Minimum horizontal stress
σ_{oct}	Octahedral normal stress
σ_v	Vertical stress
$\sigma^{\Delta T}$	Thermo-elastic stress
τ_{oct}	Octahedral shear stress

References

Aadnoy, B., Looyeh, R., 2011. Petroleum Rock Mechanics: Drilling Operations and Well Design, first ed. Gulf Professional Publishing, Houston.

Al-Ajmi, A.M., Zimmerman, R.W., 2006. Stability analysis of vertical boreholes using the Mogi-Coulomb failure criterion. Int. J. Rock Mech. Min. Sci. 43 (8), 1200–1211. http://dx.doi.org/10.1016/j.ijrmms.2006.04.001.

Detienne, J.L., Creusot, M., Kessler, N., et al., 1998. Thermally induced fractures: a field-Proven analytical model. SPE Res Eval Eng 1 (01), 30–35. SPE-30777-PA. http://dx.doi.org/10.2118/30777-PA.

Fakcharoenphol, P., Xiong, Y., Hu, L., et al., 2013. TOUGH2–EGS: a coupled geomechanical and reactive geochemical simulator for fluid and heat flow in enhanced geothermal systems. Manual. Colorado School of Mines, Golden, CO. May 2013.

Grundmann, S.R., Rodvelt, G.D., Dials, G.A., et al., 1998. Cryogenic Nitrogen as a Hydraulic Fracturing Fluid in the Devonian Shale. Presented at SPE Eastern Regional Meeting, Pittsburgh, Pennsylvania, pp. 9–11. November. SPE-51067-MS. http://dx.doi.org/10.2118/51067-MS.

Jaeger, J.C., Cook, N.G.W., Zimmerman, R., 2009. Fundamentals of Rock Mechanics, first ed. John Wiley and Sons, New York City.

King, S.R., 1983. Liquid CO2 for the Stimulation of Low-permeability Reservoirs. Presented at SPE/DOE Low Permeability Gas Reservoirs Symposium, Denver, Colordao, pp. 14–16. March. SPE-11616-MS. http://dx.doi.org/10.2118/11616-MS.

Luo, Z., Bryant, S.L., 2010. Influence of Thermo-elastic Stress on CO2 Injection Induced Fractures during Storage. Presented at SPE International Conference on CO2 Capture Storage and Utilization, New Orleans, Louisiana, pp. 10–12. November. SPE-139719-MS. http://dx.doi.org/10.2118/139719-MS.

McDaniel, B.W., Grundmann, S.R., Kendrick, W.D., et al., 1998. Field applications of cryogenic nitrogen as a hydraulic-fracturing fluid. J. Petroleum Technol. 50 (3), 38–39. SPE-38623-MS. http://dx.doi.org/10.2118/38623-MS.

Olson, J.E., Pollard, D.D., 1991. The initiation and growth of En Echelon veins. J. Struct. Geol. 13 (5), 595–608. http://dx.doi.org/10.1016/0191-8141(91)90046-L.

Wang, L., Yao, B., Cha, M., et al., 2016. 2016. Waterless fracturing technologies for unconventional reservoirs – opportunities for liquid nitrogen. J. Nat. Gas Sci. Eng. 35, 160–174. http://dx.doi.org/10.1016/j.jngse.2016.08.052.

Xiong, Y., Fakcharoenphol, P., Winterfeld, P., et al., 2013. Coupled geomechanical and reactive geochemical model for fluid and heat flow: application for enhanced geothermal reservoir. Presented at SPE Reservoir Characterization and Simulation Conference and Exhibition, Abu Dhabi, UAE, pp. 16–18. September. SPE-165982-MS. http://dx.doi.org/10.2118/165982-MS.

Zhou, X., Aydin, A., Liu, F., et al., 2010. Numerical modeling of secondary thermal fractures in hot dry geothermal reservoirs. Proc., Thirty-Fifth Work-shop on Geothermal Reservoir Engineering, Stanford, California, pp. 1–3 (Feburary).

Zhang, R., Winterfeld, P.H., Yin, X., et al., 2015. Sequentially coupled THMC model for CO2 geological sequestration into a 2D heterogeneous saline aquifer. J. Nat. Gas Sci. Eng. 27, 579–615. http://dx.doi.org/10.1016/j.jngse.2015.09.013.

Zhang, R., Yin, X., Winterfeld, P.H., et al., 2016. A fully coupled thermal-hydrological-mechanical-chemical model for CO2 geological sequestration. J. Nat. Gas Sci. Eng. 28, 280–304. http://dx.doi.org/10.1016/j.jngse.2015.11.037.

Zoback, M.D., 2007. Reservoir Geomechanics: Earth Stress and Rock Mechanics Applied to Exploration, Production and Wellbore Stability, first ed. Cambridge University Press, Cambridge.

Please cite this article in press as: Yao, B., et al., Numerical modeling of cryogenic fracturing process on laboratory-scale Niobrara shale samples, Journal of Natural Gas Science and Engineering (2016), http://dx.doi.org/10.1016/j.jngse.2016.10.041